

Universal Thermodynamics of a Strongly Interacting Fermi Gas

J. E. Thomas,¹ J. Kinast, and A. Turlapov

Physics Department, Duke University, Durham, NC 27708-0305, USA

Abstract. We study the properties of an optically-trapped, Fermi gas of ${}^6\text{Li}$ atoms, near the center of a broad Feshbach resonance, where strong interactions are observed. Strongly interacting Fermi gases exhibit universal behavior, and are of interest as models of exotic systems ranging from high temperature superconductors to neutron stars and quark-gluon plasmas. We measure the frequency and damping rate of the radial breathing mode of the trapped gas and consider quantum viscosity as a damping mechanism. We also demonstrate that the virial theorem holds and measure the heat capacity. In the experiments, energy is precisely added to the gas and an empirical temperature is determined from the spatial profiles of the cloud. Transitions are observed in both the damping rate and the heat capacity, measured as functions of the empirical temperature. Recent theory, using a pseudogap formalism, enables the first temperature calibration, and shows that the observed transition temperatures are close to that predicted for the onset of superfluidity in a strongly attractive Fermi gas.

Keywords: Fermi gas, strongly interacting, optical trap

PACS: 32.80.Pj, 03.75.Ss

1. INTRODUCTION

Since the first observation of a degenerate, strongly interacting Fermi gas [1], the field of interacting Fermi gases has made spectacular progress. Strongly interacting Fermi gases are produced in an optical trap [2], by using a magnetic field to tune a mixture of spin-up and spin-down atoms to a Feshbach resonance, where the zero energy scattering length is large compared to the interparticle spacing [1–4]. Strongly interacting Fermi gases can exhibit universal behavior and scale invariance, where the only natural length scale is the interparticle spacing. Under these conditions, the ratio of the interaction energy to the local kinetic energy is a universal parameter, denoted β [1,5]. This parameter was originally explored theoretically in the context of nuclear matter [5,6], and has now been measured by several groups [1,7–10], and found to be in reasonable agreement with recent predictions [11,12]. In the close proximity of a broad Feshbach resonance, the local thermodynamic properties of the trapped gas are believed to obey the universal hypothesis [13], i.e., they are independent of the details of the interparticle interactions, and are functions only of the density and temperature.

In the vicinity of a Feshbach resonance, pairing of spin-up and spin-down atoms occurs in the so-called crossover regime, part way between a Bose-Einstein condensate (BEC) and a Fermi superfluid comprising Cooper pairs. By tuning below resonance, Bose-Einstein

condensates (BECs) of molecular dimers have been produced from a two-component strongly interacting Fermi gas [14–17].

In contrast to studies of stable molecular BEC's, which are produced below resonance, the study and proof of superfluidity just above resonance, in the strong Cooper pairing or strongly attractive regime, has been less straightforward. Over the past two years, however, substantial evidence for superfluidity has been obtained in a variety of experiments.

Macroscopic measurements provide evidence for superfluidity in a strongly attractive Fermi gas, and provide important information on the equation of state of this universal quantum system. Evidence for superfluid hydrodynamics has been obtained in observations of anisotropic expansion after release of the cloud [1,17] and in studies of the temperature and magnetic field dependence of the frequency and damping of collective modes [18–21]. Measurements of the heat capacity [10] and collective mode damping [21] as a function of empirical temperature reveal transitions in behavior, close to the predicted superfluid transition temperature [10,12,22,23]. Recently, the observation of vortices [24] in a strongly attractive Fermi gas has provided what appears to be a definitive proof of superfluidity.

Microscopic studies of strongly attractive Fermi gases have concentrated on the detection and probing of fermionic atom pairs. Pairs were first observed by projection onto a molecular BEC [25,26]. The pair binding energy has been probed in measurements of the pairing gap, by radiofrequency spectroscopy [27] and by modulating the interaction strength [28]. In the region of a

¹ E-mail: jet@phy.duke.edu

Feshbach resonance, the pair wavefunction can contain both a dominant triplet contribution in the open collision channel, and a much smaller singlet contribution from the closed molecular channel [29,30]. Recently, molecular spectroscopy in the singlet manifold has been used to probe the molecular amplitude of the fermionic atom pairs and the superfluid order parameter throughout the Feshbach resonance region [30].

2. EXPERIMENTAL SYSTEM

We prepare a highly degenerate, strongly interacting Fermi gas of ${}^6\text{Li}$. This is accomplished using evaporation of an optically-trapped, 50-50 mixture of spin-up/down states at 840 G, just above the center of a broad Feshbach resonance [1,10,18,20,21]. To reduce the temperature, we do not employ a magnetic sweep from a BEC of molecules, in contrast to several other groups [9,17,19,24,26,27]. Instead, we evaporate directly in the strongly attractive, unitary regime: We simply exploit the large collision cross section and the rapid vanishing of the heat capacity with decreasing temperature, which is especially effective in the superfluid regime. These properties make the gas easier to cool.

In the forced evaporation, the depth of the CO_2 laser optical trap is reduced to 1/580 of its maximum value, and then recompressed to 4.6% of the maximum trap depth for most of the experiments. From the trap frequencies measured under these conditions and corrected for anharmonicity, we obtain: $\omega_\perp = \sqrt{\omega_x \omega_y} = 2\pi \times 1696(10)$ Hz, $\omega_x/\omega_y = 1.107(0.004)$, and $\lambda = \omega_z/\omega_\perp = 0.045$. Then, $\bar{\omega} = (\omega_x \omega_y \omega_z)^{1/3} = 2\pi \times 589(5)$ Hz is the mean oscillation frequency. For most of the data reported, the total number of atoms is $N = 2.0(0.2) \times 10^5$. The corresponding Fermi temperature at the trap center for a noninteracting gas is $T_F = (3N)^{1/3} \hbar \bar{\omega} / k_B \simeq 2.4 \mu\text{K}$, small compared to the final trap depth of $U_0/k_B = 35 \mu\text{K}$ (at 4.6% of the maximum trap depth). The coupling parameter of the strongly interacting gas at $B = 840$ G is $k_F a \simeq -30.0$, where $\hbar k_F = \sqrt{2mk_B T_F}$ is the Fermi momentum, and $a = a(B)$ is the zero-energy scattering length estimated from the measurements of Bartenstein et al. [31]

3. UNIVERSAL THERMODYNAMICS

As noted above, at a Feshbach resonance, a strongly interacting gas obeys the universal hypothesis, where the interparticle spacing, and hence the density n , determines the natural length scale. The local thermodynamic properties are then functions only of the density and temperature, the same variables that describe a noninteracting

Fermi gas. The universal hypothesis has directly measurable consequences, some of which we will describe briefly.

3.1. Spatial Distribution and Fermi Temperature

At zero temperature, the local energy per particle for a resonantly interacting gas is just $(3/5)(1 + \beta) \epsilon_F(n)$ where $\epsilon_F(n) = \hbar^2(3\pi^2 n)^{2/3}/(2m)$ is the local Fermi energy of a noninteracting Fermi gas and β is a universal constant [1,5,7].

For such a zero temperature gas, the net effect of the interactions is then equivalent to changing the bare mass m to an effective mass [6,10], $m^* = m/(1 + \beta)$. The equation of state then yields precisely a zero temperature Thomas-Fermi profile, $n_0(\mathbf{x})$, for which the Fermi radii are altered from those of a noninteracting gas by a factor of $(1 + \beta)^{1/4}$ [7]. Hence, the spatial distribution of the trapped gas is determined quite generally for a very low temperature cloud. We find that the measured spatial profiles of the cloud assume nearly the shape of a zero-temperature Thomas-Fermi profile [1,7,32]. Measurements of the cloud radii can then be used to determine β [7,9,10].

The Fermi temperature for a harmonically trapped, noninteracting gas, is given by $T_F = (3N)^{1/3} \hbar \bar{\omega} / k_B$. Since the effective mass for the strongly interacting gas is given by $m^* = m/(1 + \beta)$, the effective oscillation frequency is altered by a factor of $\sqrt{1 + \beta}$, and the Fermi temperature for the strongly interacting gas is given by

$$T_F' = T_F \sqrt{1 + \beta}. \quad (1)$$

3.2. Universal Hydrodynamics

At zero temperature, the local pressure of the trapped gas differs from the Fermi pressure of a noninteracting gas by a factor of $1 + \beta$ and the pressure then scales as $n^{5/3}$. In this case, upon release from a harmonic trap, the expansion dynamics are governed precisely by a scale transformation, where the density evolves according to $n(\mathbf{x}, t) = n_0(\tilde{\mathbf{x}})/\Gamma$, where $\tilde{x} = x/b_x(t)$, $\Gamma = b_x b_y b_z$, and $b_i(t)$ is a hydrodynamic expansion factor [1,33]. The predicted hydrodynamic expansion for release from a cigar-shaped trap is highly anisotropic, and independent of β , i.e., the gas expands rapidly in the originally narrow direction while remaining nearly stationary in the long direction as observed in experiments [1].

The breathing mode frequencies take on universal values when the local pressure scales as $n^{5/3}$, and are independent of β . For a cylindrically-symmetric trap, the

radial breathing mode frequency for a zero temperature gas is given by

$$\omega_{hydro} = \sqrt{\frac{10}{3}} \omega_{\perp} = 1.83 \omega_{\perp}. \quad (2)$$

For the conditions of our trap, which deviate slightly from cylindrical symmetry, exact diagonalization of the linearized hydrodynamic equations yields $\omega_{hydro} = 1.84 \omega_{\perp}$. This result is in very good agreement with our measurements [18,20,21], as shown in § 6.

One can generalize these arguments to show that they hold at all temperatures where the gas expands hydrodynamically *under isentropic conditions* [34].

3.3. Virial Theorem

According to the universal hypothesis, the local pressure P must be a function of the local density and temperature [13]. In this case, a strongly interacting Fermi gas must obey the virial theorem for a noninteracting gas at all temperatures, as we now show. One can readily show by elementary thermodynamic arguments that if $P = P(n, T)$, then

$$P = \frac{2}{3} \varepsilon(\mathbf{x}), \quad (3)$$

where $\varepsilon(\mathbf{x})$ is the local energy density, i.e., the sum of the local kinetic and interaction energies [13,34].

Balance of the pressure and trapping forces in a harmonic potential requires that $N\langle U \rangle = (3/2) \int d^3\mathbf{x} P(\mathbf{x})$, where $\langle U \rangle$ is the average potential energy per particle. Using $\int d^3\mathbf{x} \varepsilon(\mathbf{x}) = E - N\langle U \rangle$, one obtains [34]

$$N\langle U \rangle = \frac{E}{2}. \quad (4)$$

This result is remarkable: Analogous to an ideal noninteracting gas, a trapped, strongly interacting, unitary gas, comprising condensed superfluid pairs, noncondensed pairs, and unpaired atoms, should obey the virial theorem. Since $\langle U \rangle \propto \langle x^2 \rangle$, the mean square transverse radius $\langle x^2 \rangle$ of the trapped cloud should scale linearly with the total energy, as verified in our experiments, see § 4.2.

4. TOOLS FOR THERMODYNAMIC MEASUREMENTS

Equilibrium thermodynamic properties of the trapped gas, as well as dynamical properties, can be measured as functions of the temperature or of the total energy. The temperature is changed by adding energy to the gas at fixed total atom number and fixed magnetic field, starting

from the lowest temperature samples. In the following, we describe first a method for precisely adding a known energy to the gas. Then we describe a method for associating an empirical temperature with the spatial profile of the gas, and a temperature calibration method using theoretically predicted spatial profiles [35].

4.1. Precision Energy Input

Energy is added to the gas by abruptly releasing the cloud and then recapturing it after a short expansion time t_{heat} . During the expansion time, the total kinetic and interaction energy is conserved. When the trapping potential $U(\mathbf{x})$ is reinstated, the potential energy of the expanded gas is larger than that of the initially trapped gas, increasing the total energy. After waiting for the cloud to reach equilibrium, the sample is ready for subsequent measurements.

After recapture, the increase in the total energy, ΔE , is given by

$$\Delta E = \int d^3\mathbf{x} [n(\mathbf{x}, t_{heat}) - n_0(\mathbf{x})] U(\mathbf{x}), \quad (5)$$

where n_0 is the initial spatial distribution, and n is the spatial distribution after expansion during the time t_{heat} , as described in § 3.2.

For a harmonically trapped cloud which is initially at nearly zero temperature, the total energy is close to that of the ground state, which is $3/4$ of the Fermi energy per particle, i.e., $E_0 = (3/4)k_B T_F \sqrt{1 + \beta}$. The energy after expansion and recapture is given by

$$E = E_0 \left[\frac{2}{3} + \frac{b_x^2(t_{heat}) + b_y^2(t_{heat})}{6} \right]. \quad (6)$$

Equation 6 has a simple physical interpretation. After release from a harmonic trap, and subsequent recapture after a time t_{heat} , the potential energy in each transverse direction is increased as the square of the expansion factors, b_x and b_y , where $b_z(t_{heat}) \simeq 1$, for the conditions of our experiments. The total potential energy is half of the total energy, since the unitary gas obeys the virial theorem for an ideal gas at all temperatures, as shown in § 4.2. Hence, the initial potential energy in each direction is $1/6$ of the total energy. Note that, by using Eq. 5, the corrections to the energy change arising from trap anharmonicity are readily determined [10].

4.2. Test of the Virial Theorem

To test the virial theorem prediction, the gas is evaporatively cooled to the lowest temperature and then the

energy is increased as described above. For each value of t_{heat} , E is calculated according to Eq. 6. For each final energy, the gas is released and the transverse radius of the cloud is measured after a *fixed* expansion time of 1 ms. The observed linear scaling of $\langle x^2 \rangle$ with the calculated E , Fig. 1 verifies the virial theorem prediction. The linear scaling of $\langle x^2 \rangle$ with E also confirms that the expansion dynamics is closely hydrodynamic at all temperatures, since $\langle x^2 \rangle$ is measured after a fixed expansion time for all energies, which implies that the expansion factor must be nearly the same over the range of temperatures studied.

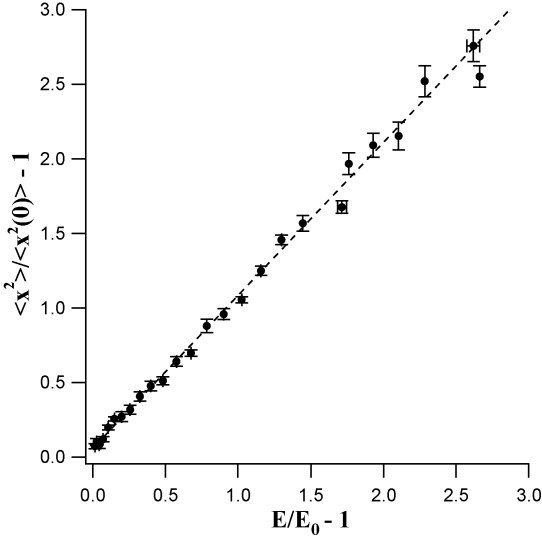


FIGURE 1. $\langle x^2 \rangle / \langle x^2(0) \rangle$ versus E/E_0 for a unitary gas of ${}^6\text{Li}$, showing linear scaling, and verifying the virial theorem prediction. Here $\langle x^2 \rangle$ is the measured transverse mean square size. E is the total energy, calculated using Eq. 6. E_0 and $\langle x^2(0) \rangle$ denote the ground state values.

4.3. Empirical Temperature Measurement

Measurement of temperature in a noninteracting or weakly interacting Fermi gas is readily accomplished by fitting a Thomas-Fermi (T-F) distribution to the spatial profile of the cloud either in the trap, or after ballistic expansion, which alters the profile by a scale factor [1,33]. We normally integrate the measured column density of the expanded cloud over the axial dimension, and obtain the spatial profile in one transverse dimension, $n_{TF}(x; \sigma_x, T/T_F)$. The spatial profile is taken to be a function of two parameters, the Fermi radius σ_x , i.e., the cloud radius at zero temperature, and the reduced temperature T/T_F , i.e., the ratio of the Boltzmann temperature T to the trap Fermi temperature for a noninteracting gas, T_F .

One can consider $\sigma_x = \sqrt{2k_B T_F / (m\omega_x^2)}$ to set the length scale of the spatial profile and T/T_F as a shape parameter. At low T/T_F , the shape approaches a zero temperature T-F profile, $\propto (1 - x^2/\sigma_x^2)^{5/2}$, while at high T/T_F , the profile approaches a Maxwell-Boltzmann shape $\propto \exp[-m\omega_x^2 x^2 / (2k_B T)] = \exp[-(x^2/\sigma_x^2)(T_F/T)]$.

In the latter case, only the product of T/T_F and σ_x^2 appears. Hence, for determination of the reduced temperature, it is convenient to determine the Fermi radius from the lowest temperature data, and then to hold this radius constant, i.e., to take $\sigma_x = c_x N^{1/6}$ in subsequent measurements at higher temperature, where c_x is held constant. In this way, the reduced temperature T/T_F is uniquely correlated with (and can be used to parametrize) the shape of the spatial profile.

For a unitary gas, the spatial profile is not precisely known, and there are no simple analytical formulae except at $T = 0$, where the equation of state assures that the shape of the cloud must take the zero temperature T-F form, with $\sigma_x \rightarrow \sigma'_x$, where $\sigma'_x = \sigma_x (1 + \beta)^{1/4}$, as discussed above [7]. We obtain β by comparing the transverse radius of the trapped cloud for the interacting gas with that of the noninteracting gas [7]. For the noninteracting gas, we use either the calculated σ_x or the radius measured after ballistic expansion. For the interacting gas, we obtain σ'_x after hydrodynamic expansion for 1 ms. We find that $\beta = -0.49(0.04)$ (statistical error only). Similar results are obtained by measurements on the axial dimension of the trapped cloud without expansion [9] and by direct measurements of the interaction energy [8]. The discrepancy between the measurements may arise from the sensitivity of β to the precise location of the Feshbach resonance [9], which in ${}^6\text{Li}$ has been most recently measured by radiofrequency methods [31].

Although the spatial profile of a unitary gas is not precisely known, we observe experimentally that the binned, one-dimensional shape is closely approximated by a T-F profile for a noninteracting gas. Further, recent theoretical predictions of the spatial profile [35] show that the shape is nearly of the T-F form at all temperatures, as a consequence of the existence of preformed pairs. Hence, to provide a parametrization of the spatial profiles, we define an *empirical* reduced temperature $\tilde{T} \equiv (T/T_F)_{fu}$, and take the one dimensional spatial profile of the cloud to be of the form $n_{TF}(x; \sigma'_x, \tilde{T})$.

In general, the empirical reduced temperature does not directly determine the reduced temperature T/T_F . However, at $T = 0$, the T-F shape is exact, so that $\tilde{T} = 0$ coincides with $T/T_F = 0$. Hence, the procedure for determining σ'_x from the data at very low temperature, where $\tilde{T} \simeq 0$, is consistent, i.e., we take $\sigma'_x = c'_x N^{1/6}$, where c'_x is a constant.

Further, at sufficiently high temperature, the

cloud profile must have a Maxwell-Boltzmann form $\propto \exp[-m\omega_x^2 x^2 / (2k_B T)] = \exp[-(x^2 / \sigma_x'^2)(1/\tilde{T})]$. This determines the natural reduced temperature scale, \tilde{T}_{nat} ,

$$\tilde{T}_{nat} = \frac{T}{T_F \sqrt{1 + \beta}}, \quad (7)$$

which follows from the interacting gas Fermi radius, $\sigma_x' = \sigma_x (1 + \beta)^{1/4}$, and the definition of the noninteracting gas Fermi radius σ_x .

The empirical temperature scale is therefore exact at $T = 0$ and at high temperature, for a fixed interacting gas Fermi radius (which determines β). To calibrate \tilde{T} more generally, we fit profiles of the form $n_{TF}(x; \sigma_x', \tilde{T})$ to the spatial profiles predicted as a function of T/T_F using a pseudogap formalism [10,35]. The value of σ_x' is determined from the lowest temperature theoretical profile, and \tilde{T} is determined for all of the predicted profiles.

If the natural temperature were the correct scale at all T , then one would expect $T/T_F = \tilde{T} \sqrt{1 + \beta} = 0.71 \tilde{T}$. Remarkably, above the predicted superfluid transition temperature, where $T_c/T_F = 0.29$, i.e., for $\tilde{T} \geq 0.45$, the natural temperature scale is in close agreement with predictions [10], even though noncondensed pairs are believed to exist up to at least $T/T_F \simeq 0.6$, and are present in the predicted profiles. However, below the transition, for $0 < T \leq 0.29$, i.e., for $0 \leq \tilde{T} \leq 0.45$, we find that there is a systematic deviation: Here, $T/T_F = 0.54 \tilde{T}^{2/3}$, and the natural temperature scale underestimates the reduced temperature [10]. This is reasonable, since the energy of the unitary gas, and hence the mean square cloud size, increases as a higher power of T/T_F than quadratic. The full empirical temperature calibration is shown in the inset in Fig. 3.

5. HEAT CAPACITY

The techniques of precision energy input and empirical temperature measurement provide a method for exploring the heat capacity [10,32] of a strongly interacting Fermi gas. In the experiments, the ${}^6\text{Li}$ gas is cooled to very low temperature, $\tilde{T} \simeq 0.04$, by forced evaporation at 840 G, just above the center of the Feshbach resonance, as described above. Then, the gas is heated by adding a known energy. Finally, the gas is released from the trap and allowed to expand for 1 ms. As observed above, the gas expands hydrodynamically by a scale factor, so that the shape of the expanded cloud closely approximates that of the trapped cloud, enabling a determination of \tilde{T} .

Figure 2 shows that the reduced energy of the gas, E/E_0 , scales with empirical temperature $\tilde{T} = (T/T_F)_{fit}$ in much the same way as that of an ideal, noninteracting, Fermi gas. However, closer examination reveals that the

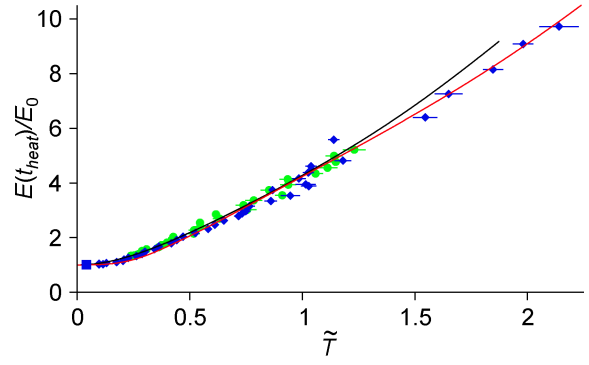


FIGURE 2. Total energy versus temperature. For each heating time t_{heat} , the temperature parameter \tilde{T} is measured from the cloud profile, and the total energy $E(t_{heat})$ is calculated from Eq. 6 in units of the ground state energy E_0 . Circles: noninteracting Fermi gas data; Diamonds: strongly interacting Fermi gas data. Upper solid curve: predicted energy versus reduced temperature for a noninteracting, trapped Fermi gas, $E_{ideal}(\tilde{T})/E_{ideal}(0)$; Lower solid curve: predicted energy versus \tilde{T} for the unitary case. No temperature calibration is applied since $\tilde{T} \approx \tilde{T}_{nat}$ over the broad temperature range shown. Note that the lowest temperature point (solid square) is constrained to lie on the upper noninteracting gas curve.

low temperature data is better fit by a power law in \tilde{T} than by the ideal gas scaling. The same data on a $\log - \log$ plot shows a transition in behavior [10,32].

By using the temperature calibration, and replotting the raw data as in Fig. 3, we find that the transition occurs at $T/T_F = 0.27$, in very good agreement with the prediction for the superfluid transition, $T_c/T_F = 0.29$ [10]. We also find that the behavior of the energy with temperature is in very good agreement with the predictions [10].

By fitting a power law in T/T_F to the data above and below the transition temperature, we obtain analytic approximations to the energy $E(T/T_F)$, from which the heat capacity is calculated using $C = (\partial E / \partial T)_{N,U}$, where the number N and trap depth U are constant in the experiments. For $T/T_F \leq 0.27$, we obtain $E/E_0 - 1 = 97.3 (T/T_F)^{3.73}$, while for $T/T_F \geq 0.27$, $E/E_0 - 1 = 4.98 (T/T_F)^{1.43}$. By differentiating the energy in each region with respect to T , we find that the heat capacity exhibits a jump at the transition temperature, comparable in size to that expected for a transition between a superfluid and a normal fluid [10].

The appearance of a transition in the behavior in the heat capacity, i.e., in the behavior of the energy versus temperature, is model-independent, as it appears in the empirical temperature data, $E(\tilde{T})/E_0$, without calibration [32]. However, the estimate of the transition temperature T_c/T_F and the magnitude of the jump in heat capacity are model-dependent, since the temperature estimates are obtained by calibration using the theoretical spatial profiles.

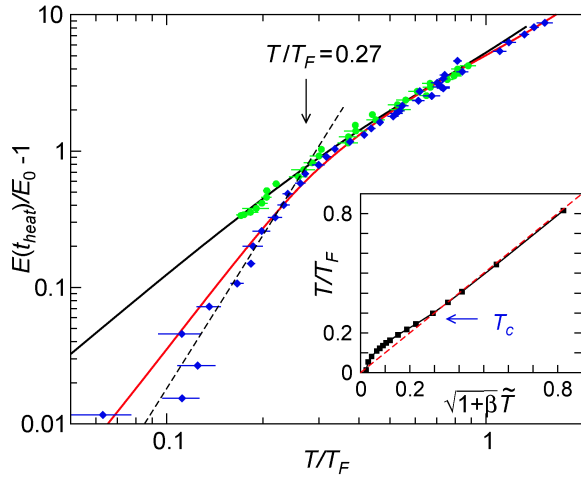


FIGURE 3. Energy input versus temperature from Fig. 2 after temperature calibration, on a $\log - \log$ scale. The strongly interacting Fermi gas shows a transition in behavior near $T/T_F = 0.27$. Circles: noninteracting Fermi gas data; Diamonds: strongly interacting Fermi gas data; Lower (upper) solid curves: prediction for a unitary (noninteracting), trapped Fermi gas, calculated at trap depth $U_0/E_F = 14.6$ as in the experiments; Dashed line: best fit power law $97.3 (T/T_F)^{3.73}$ to the calibrated unitary data for $T/T_F \leq 0.27$. The inset shows the calibration curve, which has been applied to the unitary data (diamonds). The diagonal dashed line in the inset represents $T/T_F = \sqrt{1 + \beta} \tilde{T}$. Here $E_0 \equiv E(T = 0)$, and $E_F = k_B T_F$ is the noninteracting gas Fermi energy.

6. COLLECTIVE OSCILLATIONS

As the determination of the transition temperature in the crossover regime is of great interest, we look for corresponding transitions in the mechanical properties of the gas. In this section, we describe our comprehensive measurements of the temperature dependence of the frequency and damping of the radial breathing mode [21]. The temperature is increased by adding energy to the gas. Then, the empirical temperature is measured from the spatial profiles of the released cloud as described above.

The radial breathing mode is excited by releasing the gas from the trap for a short time and then recapturing the cloud. In contrast to the method used to add energy, the gas is not allowed to thermalize, and the expansion time, $25 \mu\text{s}$, is so short that the energy increase is negligible. After recapture, the cloud is allowed to oscillate in the trap for a variable time, t_{hold} after which it is released and imaged as described above.

The width of the cloud, Fig. 4, oscillates at a frequency ω . The oscillation amplitude decays at a rate $1/\tau$. To determine ω and τ , we fit a damped sinusoid to the mean square width as a function of t_{hold} .

From the measured values of the trap oscillation frequencies, we predict the radial breathing frequency for a

noninteracting gas $\omega_{\text{nonint}} = 2\omega_x = 2.10\omega_{\perp}$ and the hydrodynamic frequency for a strongly interacting (unitary) gas, $\omega_{\text{hydro}} = 1.84\omega_{\perp}$, as given in § 3.2.

Figure 5 shows the measured frequency ω in units of ω_{\perp} , as a function of temperature. Remarkably, after correction for anharmonicity, the frequency is very close to the hydrodynamic value, and far from the collisionless (ballistic) value over the entire range of temperatures explored. This behavior suggests that the gas oscillates under conditions which are close to locally isentropic [34].

In contrast to the frequency, the damping rate, Fig. 6, shows a transition in behavior at $\tilde{T} \simeq 0.5$. For empirical temperatures in the range $0 \leq \tilde{T} \leq 0.5$, the data is well fit by a line (0.998 correlation coefficient), while above 0.5, the damping rate behaves quite differently, exhibiting non-monotonic behavior. The value of $\tilde{T} = 0.5$ lies just above the predicted superfluid transition temperature, where $\tilde{T} \simeq \tilde{T}_{\text{nat}}$ is a good approximation. Using Eq. 7, we find that $\tilde{T} = 0.5$ corresponds to $T/T_F = 0.35$. This is quite close to the value measured for the transition in the heat capacity, $T/T_F = 0.27$, and is consistent with recent predictions, $T_c/T_F = 0.29$ [22,32], $T_c/T_F = 0.31$ [36], and $T_c/T_F = 0.30$ [23].

The damping rate also appears to have a plateau and a further increase near $\tilde{T} = 1.0$, i.e., $T/T_F = 0.71$, close to the region where the pairing gap is comparable to the collective mode quantum, $\hbar\omega$. This behavior may arise from the breaking of weakly bound pairs in this temperature region.

6.1. Quantum Viscosity

In a unitary Fermi gas, there is a natural unit of viscosity, η which is determined by the interparticle spacing, L . Viscosity has dimensions of momentum/area. Hence, $\eta \simeq \hbar/L^3 \propto \hbar n$, where n is the local density. Since $\eta \propto \hbar$, we consider this scale as the natural unit of quantum viscosity. Following Gelman et al. [37], we take

$$\eta = \alpha \hbar n, \quad (8)$$

where α is a dimensionless constant.

It is instructive to determine α from the lowest damping rates observed in measurements of the breathing mode. For the axial mode measured by the Innsbruck group [19], the axial damping ratio is found to be very small, $1/(\omega_z \tau_z) = 1.5 \times 10^{-3}$. This corresponds to observed axial damping times of several seconds, since $\omega_z = 2\pi \times 22.5$ Hz. For the radial breathing mode measured by the Duke group [20,21], the damping ratio is $1/(\omega_{\perp} \tau_{\perp}) = 1.3 \times 10^{-2}$, corresponding to damping times of up to seven milliseconds. Similar results are obtained by the Innsbruck group [19].

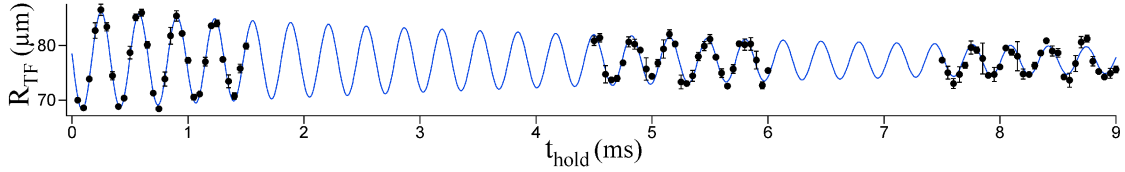


FIGURE 4. Radial breathing mode amplitude versus hold time.

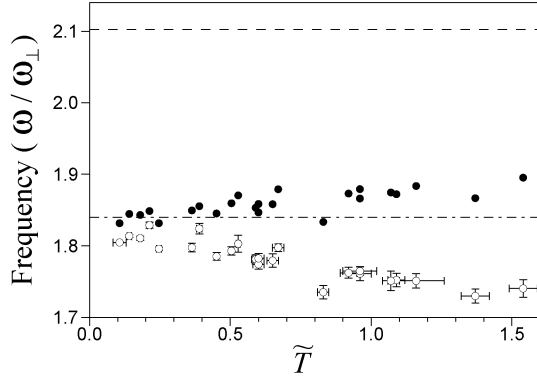


FIGURE 5. Frequency ω versus empirical reduced temperature \tilde{T} . Open circles—measured frequencies; Black dots—after correction for anharmonicity using a finite-temperature Thomas-Fermi profile. The dot-dashed line is the unitary hydrodynamic frequency $\omega_H = 1.84\omega_\perp$, for our trap parameters. The dashed line at the top of the scale is the frequency $2\omega_\perp = 2.10\omega_\perp$ observed for a noninteracting gas at the lowest temperatures.

To determine α , we introduce a pressure term which arises from the shear viscosity [38], into the hydrodynamic equations for a compressible fluid. For low damping, the gas can be assumed to oscillate under nearly isentropic conditions at all temperatures [34]. In this case, the local stream velocity components are of the form $u_i = x_i \dot{b}_i / b_i$, where $b_i(t)$ is a scale factor [33,39]. The spatial derivatives of the stream velocity, which determine the shear pressure, are therefore spatially independent, and the gradient of the viscosity determines the spatial dependence of the shear pressure. The equations of motion for the b_i are readily solved and yield for the radial mode,

$$\frac{1}{\omega_\perp \tau_\perp} = \frac{4}{3} \frac{\alpha}{(3N\lambda)^{1/3} \sqrt{1+\beta}}, \quad (9)$$

and for the axial mode,

$$\frac{1}{\omega_z \tau_z} = \frac{16}{5} \frac{\alpha \lambda}{(3N\lambda)^{1/3} \sqrt{1+\beta}}. \quad (10)$$

Equation 10 predicts that the axial damping ratio is smaller than that of the radial mode by a factor of $\lambda \equiv$

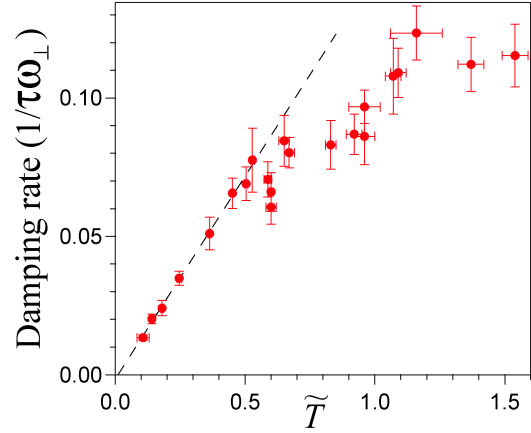


FIGURE 6. Temperature dependence of the damping rate for the radial breathing mode of a trapped ${}^6\text{Li}$ gas at 840 G, showing a transition in behavior. The dashed line shows fit to a line which extrapolates close to zero at zero temperature.

$\omega_z / \omega_\perp \ll 1$. Assuming $\beta \simeq -0.5$ [32], and using the measurements for the damping ratio of axial mode by the Innsbruck group, where $N = 4 \times 10^5$, and $\lambda = 0.03$, we obtain from Eq. 10, $\alpha = 0.4$. Using the parameters for our radial mode experiments, where $N = 2 \times 10^5$, we obtain $\alpha = 0.2$. From these results, we conclude that the measured damping ratios are comparable to those expected for the quantum viscosity scale.

Eqs. 9 and 10 also predict that the damping ratios should decrease as $N^{-1/3}$ with increasing total atom number N . However, we find experimentally that the data are nearly independent of N for fixed nonzero \tilde{T} : Decreasing the number of atoms N by a factor of 3 produces damping ratios which lie on the linear extrapolation for N atoms [21]. Hence, the observed damping ratios are consistent with the quantum viscosity scale, but viscosity may not be the cause of the damping.

7. CONCLUSIONS

We have studied a highly-degenerate, strongly interacting Fermi gas, which is prepared by direct evaporation at a Feshbach resonance in an optical trap. By precisely

adding energy to the gas, we have verified that the virial theorem holds, despite strong interactions. Using an empirical temperature parameter linked to the cloud profiles, we observe transitions in both the heat capacity and in the damping rate of the radial breathing mode. The observation of these transitions is model independent, but the method used to calibrate the temperature scale is model dependent. Nevertheless, the two measured transition temperatures are consistent, and in good agreement with predictions of the superfluid transition temperature in the unitary regime.

ACKNOWLEDGMENTS

This research is supported by the Army Research Office and the National Science Foundation, the Physics for Exploration program of the National Aeronautics and Space Administration, and the Chemical Sciences, Geosciences and Biosciences Division of the Office of Basic Energy Sciences, Office of Science, U. S. Department of Energy.

REFERENCES

1. K. M. O'Hara, S. L. Hemmer, M. E. Gehm, S. R. Granade, and J. E. Thomas, *Science*, **298**, 2179 (2002).
2. J. E. Thomas, and M. E. Gehm, *Am. Scientist*, **92**, 238 (2004).
3. M. Houbiers, R. Ferwerda, H. T. C. Stoof, W. I. McAlexander, C. A. Sackett, and R. G. Hulet, *Phys. Rev. A*, **56**, 4864 (1997).
4. M. Houbiers, H. T. C. Stoof, W. I. McAlexander, and R. G. Hulet, *Phys. Rev. A*, **57**, R1497 (1998).
5. H. Heiselberg, *Phys. Rev. A*, **63**, 043606 (2001).
6. G. A. Baker, Jr., *Phys. Rev. C*, **60**, 054311 (1999).
7. M. E. Gehm, S. L. Hemmer, S. R. Granade, K. M. O'Hara, and J. E. Thomas, *Phys. Rev. A*, **68**, 011401(R) (2003).
8. T. Bourdel, J. Cubizolles, L. Khaykovich, K. M. F. Magälhaes, S. Kokkelmans, G. V. Shlyapnikov, and C. Salomon, *Phys. Rev. Lett.*, **91**, 020402 (2003).
9. M. Bartenstein, A. Altmeyer, S. Riedl, S. Jochim, C. Chin, J. H. Denschlag, and R. Grimm, *Phys. Rev. Lett.*, **92**, 120401 (2004).
10. J. Kinast, A. Turlapov, J. E. Thomas, Q. Chen, J. Stajic, and K. Levin, *Science*, **307**, 1296 (2005), published online 27 January 2005 (10.1126/science.1109220).
11. J. Carlson, S.-Y. Chang, V. R. Pandharipande, and K. E. Schmidt, *Phys. Rev. Lett.*, **91**, 050401 (2003).
12. A. Perali, P. Pieri, and G. C. Strinati, *Phys. Rev. Lett.*, **93**, 100404 (2004).
13. T.-L. Ho, *Phys. Rev. Lett.*, **92**, 090402 (2004).
14. S. Jochim, M. Bartenstein, A. Altmeyer, G. Hendl, S. Riedl, C. Chin, J. H. Denschlag, and R. Grimm, *Science*, **302**, 2101 (2003).
15. M. Greiner, C. A. Regal, and D. S. Jin, *Nature*, **426**, 537 (2003).
16. M. W. Zwierlein, C. A. Stan, C. H. Schunck, S. M. F. Raupach, S. Gupta, Z. Hadzibabic, and W. Ketterle, *Phys. Rev. Lett.*, **91**, 250401 (2003).
17. T. Bourdel, L. Khaykovich, J. Cubizolles, J. Zhang, F. Chevy, M. Teichmann, L. Tarruell, S. Kokkelmans, and C. Salomon, *Phys. Rev. Lett.*, **93**, 050401 (2004).
18. J. Kinast, S. L. Hemmer, M. E. Gehm, A. Turlapov, and J. E. Thomas, *Phys. Rev. Lett.*, **92**, 150402 (2004).
19. M. Bartenstein, A. Altmeyer, S. Riedl, S. Jochim, C. Chin, J. H. Denschlag, and R. Grimm, *Phys. Rev. Lett.*, **92**, 203201 (2004).
20. J. Kinast, A. Turlapov, and J. E. Thomas, *Phys. Rev. A*, **70**, 051401(R) (2004).
21. J. Kinast, A. Turlapov, and J. E. Thomas, *Phys. Rev. Lett.*, **94**, 170404 (2005).
22. Q. Chen, J. Stajic, and K. Levin, *Phys. Rev. Lett.*, **95**, 260405 (2005).
23. P. Massignan, G. M. Bruun, and H. Smith, *Phys. Rev. A*, **71**, 033607 (2005).
24. M. Zwierlein, J. Abo-Shaeer, A. Schirotzek, C. Schunck, and W. Ketterle, *Nature*, **435**, 1047 (2005).
25. C. A. Regal, M. Greiner, and D. S. Jin, *Phys. Rev. Lett.*, **92**, 040403 (2004).
26. M. W. Zwierlein, C. A. Stan, C. H. Schunck, S. M. F. Raupach, A. J. Kerman, and W. Ketterle, *Phys. Rev. Lett.*, **92**, 120403 (2004).
27. C. Chin, M. Bartenstein, A. Altmeyer, S. Riedl, S. Jochim, J. H. Denschlag, and R. Grimm, *Science*, **305**, 1128 (2004).
28. M. Greiner, C. A. Regal, and D. S. Jin, *Phys. Rev. Lett.*, **94**, 070403 (2005).
29. G. M. Falco, and H. T. C. Stoof, *Phys. Rev. Lett.*, **92**, 130401 (2004).
30. G. B. Partridge, K. E. Strecker, R. I. Kamar, M. W. Jack, and R. G. Hulet, *Phys. Rev. Lett.*, **95**, 020404 (2005).
31. M. Bartenstein, A. Altmeyer, S. Riedl, R. Geursen, S. Jochim, C. Chin, J. H. Denschlag, R. Grimm, A. Simoni, E. Tiesinga, C. J. Williams, and P. S. Julienne, *Phys. Rev. Lett.*, **94**, 103201 (2005).
32. J. Kinast, A. Turlapov, and J. E. Thomas, Heat capacity of a strongly-interacting Fermi gas (2004), arXiv:cond-mat/0409283.
33. C. Menotti, P. Pedri, and S. Stringari, *Phys. Rev. Lett.*, **89**, 250402 (2002).
34. J. E. Thomas, A. Turlapov, and J. Kinast, *Phys. Rev. Lett.*, **95**, 120402 (2005).
35. J. Stajic, Q. Chen, and K. Levin, *Phys. Rev. Lett.*, **94**, 060401 (2005).
36. A. Perali, P. Pieri, L. Pisani, and G. C. Strinati, *Phys. Rev. Lett.*, **92**, 220404 (2004).
37. B. A. Gelman, E. V. Shuryak, and I. Zahed, Cold strongly coupled atoms make a near-perfect liquid (2005), arXiv:nucl-th/0410067.
38. L. D. Landau, and E. M. Lifshitz, *Fluid Mechanics*, Pergamon Press, New York, 1975.
39. D. Guéry-Odelin, F. Zambelli, J. Dalibard, and S. Stringari, *Phys. Rev. A*, **60**, 4851 (1999).